Damage at high strain rates in semi-crystalline polymers

Romain Balieu, Franck Lauro, Bruno Bennani, Grégory Haugou, Fahmi Chaari, Tsukatada Matsumoto, Ernesto Mottola

International Journal of Impact Engineering 76 (2015) 1-8

Damage at high strain rates in semi-crystalline polymers

R. Balieu [a, *], F. Lauro [b], B. Bennani [b], G. Haugou [b], F. Chaari [b], T. Matsumoto [c], E. Mottola [c]

[a] Division of Highway and Railway Engineering, KTH Royal Institute of Technology, SE-10044 Stockholm, Sweden
[b] Laboratory of Industrial and Human Automation Control, Mechanical Engineering and Computer Sciences, LAMIH-UMR CNRS 8201, University of Valenciennes, Le Mont Houy, Bat. CISIT, 59313 Valenciennes Cedex 9, France
[c] TOYOTA MOTOR EUROPE, B-1140 Brussels, Belgium

ABSTRACT

A specific damage characterization method using Digital Image Correlation for semi-crystalline polymers is proposed for a wide range of strain rates. This damage measurement is an extension of the SE Ė method [16] which was developed to characterize the behaviour laws at constant strain rates of polymeric materials. This procedure is compared to the well-known damage characterization by loss of stiffness technique under quasi-static loading. In addition, an in-situ tensile test, carried out in a microtomograph, is used to observe the cavitation phenomenon in real time. The different ways used to evaluate the damage evolution are compared and the proposed technique is also suitable for measuring the ductile damage observed in semi-crystalline polymers under dynamic loading.

Keywords:
Damage
Digital image correlation Microtomograph
Semi-crystalline polymers
High strain rates

1. Introduction

Semi-crystalline polymers have a complex behaviour which depends on several parameters, such as temperature, pressure and strain rate, and they are often accompanied by volume change during their viscoplastic deformations [1,2]. This complex behaviour has led to the development of several material models in which these parameters are taken into account to describe the deformation process until failure. Ahzi et al. [3] and Ayoub et al. [4,5] proposed physical constitutive models for semi-crystalline polymers where the intermolecular resistance is treated in a composite framework. In these models, the crystalline and amorphous phases are considered as two separate resistances. Following this microstructure, some multi-scale constitutive models have also been developed to capture their viscoelastic, viscoplastic behaviour [6,7]. Finally, models based on the continuum mechanics and overstress approach have also been developed in static [8,9] and furthermore, extended by taking the degree of crystallinity into account [10]. These models were also proposed for dynamic applications as they are easier to implement into finite element codes as they accurately describe the large deformation process of polymers [2,11–13].

Nevertheless, all these models need material parameters which are sometimes difficult to identify due to their nature or the early necking stage in the deformation process. As a consequence, specific methods have been developed to obtain information after necking by using constant strain rate control with a video-controlled system [14,15] or by using full-field data from digital correlation measurement from heterogeneous displacement fields [16]. With the first method the speed loading is controlled according to real time deformation and then limited to quasi-static tests. The second method was then developed to overcome this problem and applied to dynamic tensile tests. They both give very good results to obtain stress-strain relations at constant strain rate. However, the damage measurement is still a challenge on a large strain rate range. G'sell [17] first proposes an extension of his method, by measuring a volume variation with seven spots painted on the tensile specimen to follow the deformation in the plane and considering transverse isotropy for the thickness direction [18]. Once again, this method is limited to quasi-static cases and the significant volume considered could lead to a mean damage value. The classical loss of stiffness technique could also be used by measuring the Young modulus variation with loading–unloading curves but it is also limited to quasi-static conditions [19]. Finally, inverse approaches could be used to identify parameters of damage models, nevertheless they are always based on macroscopic mechanical data which induces less accuracy [20,21]. In this paper, the SEĖ method [16], which was first developed for the polymer

DOI : 10.1016/j.ijimpeng.2014.08.013

behaviour identification on a large strain rate range, is extended to the damage measurement on a large strain rate range. This method is applied to a polypropylene filled with 20% wt of mainly talc particles called Hostacom by LyondellBasell, for various strain rates and on small volumes all along the tensile test specimen. To validate this approach, the method is first applied under quasi static loadings and compared with the loss of stiffness technique. Tensile tests inside a microtomograph are also performed to complete the validation. As good results are obtained by comparing these various techniques, the SEÈ method for damage measurement is then applied to dynamic tensile tests carried out on a hydraulic jack and Hopkinsonâ€™s bars. The results obtained for this semi-crystalline polymer filled with mineral particles highlight the independence of the damage evolution to the strain rates.

2. Damage at low strain rates

2.1. Strain field measurements by Digital Image Correlation

The SEÈ method was developed to identify the behaviour laws at constant strain rates for a large strain rate range (quasi-static to dynamic) from uniaxial constant speed tests. In this method, the Digital Image Correlation (DIC) measurement is used to identify the true stress–strain relationships of the material associated with the true strain rates (not constant) of each speed loading. It results in a true behaviour surface in the space of true strain, true stress, true strain rate. By cutting this behaviour surface at the desired strain rate, the behaviour laws at constant strain rate are therefore obtained 16. Due to the heterogeneity of the deformation along the length of the specimen, the strain and strain rate are not constant in the whole specimen. The displacement field measurements (achieved by DIC) are carried out in the Region of Interest (ROI), which is the length gauge of the tensile specimen, on each Zone of Interest (ZOI) included in the ROI (Fig. 1(a)). Various strains and strain rates measured in each ZOI are consequently obtained. The Henky in-plane strain tensor $\underline{\underline{e}}$ is deduced from the displacement fields of the ZOI. In the SEÈ method, a hypothesis about the material behaviour (incompressibility, transverse isotropy, …) has to be made to obtain the thickness strain in order to calculate the tensile stress in each ZOI by taking into account the force applied also on each ZOI. To achieve it, the resultant force is equally divided on each ZOI which have the same dimension (initially) and afterwards divided by the current section area of the ZOI (measured by DIC). Uniaxial quasi-static tensile tests on flat specimens at 1 mm/min are carried out with, two cameras in front of the specimen to follow the displacement field, and one for the measurement of the thickness variation. This procedure is used to measure the volume variation during the tests. The Henky longitudinal, transversal and thickness strains are presented in Fig. 1(b).

A transverse isotropy is observed during the tensile test as the transversal ($\mathbf{e}_{xx}$)and thickness strains ($\mathbf{e}_{zz}$) are very close, as shown in Fig. 1(b). Fig. 2 shows the true volumetric strain evolution (i.e. $\mathrm{tr}(\underline{\underline{e}})$) versus the true longitudinal strain evolution during the test. With this measurement technique, the non-isochoric viscoplastic deformation is clearly captured.

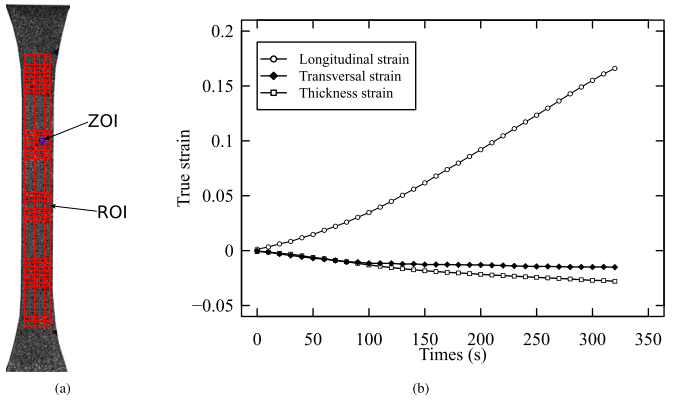

Fig. 1. Representation of the ROI divided in ZOI on the tensile specimen (a). Comparison of the true (Hencky) longitudinal ($\mathbf{e}_{xx}$), transversal $\mathbf{e}_{yy}$ and thickness $\mathbf{e}_{zz}$ strains for the tensile test at 1 mm/min (b).

2.2. Damage measurements with the SEÈ method

Damage, as well as the viscoplastic deformation, is an irreversible process which evolves during the deformation. Furthermore, the deformation of mineral filled semi-crystalline polymers induces decohesion at the charge–matrix interface. In this case, the viscoplastic response of the material is accompanied by damage in the form of nucleation, growth and coalescence of cavities. Low and high magnifications SEM micrograph of the fracture surface of mineral filled polypropylene, after a tensile loading at 1 mm/min, are shown in Fig. 3(a) and (b). A ductile fracture is observed with filament structures. The fibrillation observed is due to the cavitation phenomenon which occurs in the material. Nucleation of cavities around the mineral fillers is observed as well as growth of voids in the matrice part of the polymer.

In the Continuum Damage Mechanics approach, the damage variable D is defined by the surface density of micro-voids and micro-cracks lying on a plane cutting the Representative Volume Element (RVE) of real cross sectional area S. The RVE, introduced in mechanics of continuous media, represents a volume where all properties are represented by homogenized variables. For the plan with normal $\vec{n}$, the damage variable is given by

$$D_{(\vec{n})} = \frac{S_D}{S}, \tag{1}$$

where S_D is the effective cross sectional area which corresponds to the intersection of all micro-cracks and micro-voids lying in S. For an isotropic damage, the damage variable $D_{(\vec{n})}$ does not depend on the normal $\vec{n}$. This variable is therefore a scalar [22] such as

$$D = \frac{S_D}{S}. \tag{2}$$

By using the strain measures obtained by DIC, the true stress, which takes the reduction of the real cross-sectional area into account for each ZOI, is therefore calculated assuming the compressibility (transverse isotropy) $\sigma^{\mathrm{com}}_{yy_i}$ or the incompressibility hypothesis $\sigma^{\mathrm{com}}_{yy_i}$, such as

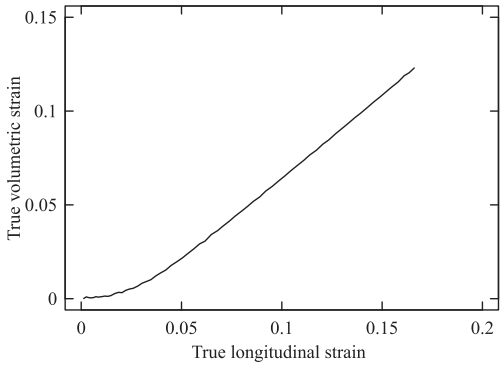

Fig. 2. True volumetric strain measured by DIC for the tensile test at 1 mm/min.

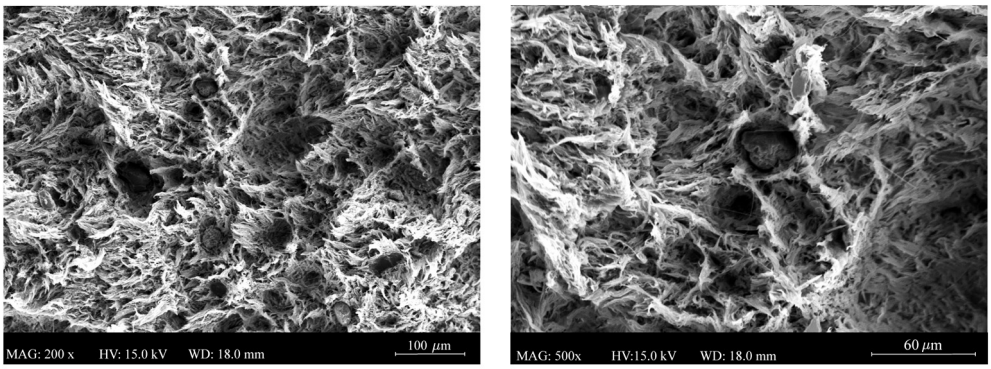

(a) (b)

Fig. 3. Low magnification SEM micrograph of the fracture surface of mineral filled polypropylene under tensile loading at 1 mm/min (a). High magnification SEM micrograph of the fracture surface of mineral filled polypropylene under tensile loading at 1 mm/min (b).

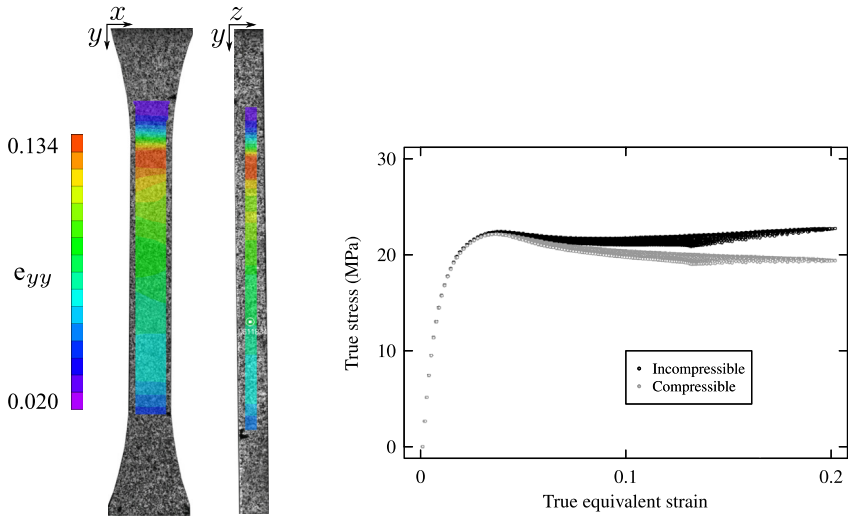

(a) (b)

Fig. 4. Tranversal and thickness strains along the specimen(a). Incompressible and compressible behaviour relationships obtained by the SEĖ method at 1 mm/min for different ZOI (b).

$$\sigma_{yy_i}^{\text{com}} = \frac{F_i}{S_{0_i}} \exp(-2e_{xx_i}), \tag{3}$$

$$\sigma_{yy_i}^{\text{inc}} = \frac{F_i}{S_{0_i}} \exp(e_{yy_i}), \tag{4}$$

where S_{0_i}, e_{xx_i}, e_{yy_i} and F_i are the initial cross section, transversal and longitudinal strains and resultant force on each ZOI subscribed by i, respectively. These different hypotheses have a strong impact on the resulting behaviour laws. Fig. 4(b) shows the true behaviour laws (compressible and incompressible) calculated with the SEĖ method for the uniaxial tensile test at 1 mm/min on different ZOI. Different stress–strain relationships are then obtained in each ZOI due to the heterogeneous strain field (Fig. 4(a)). A decrease of the stresses at increasing strains (softening) is observed with the compressible assumption. On the other hand, the incompressible hypothesis produces an increase in stresses at increasing strains (hardening) on the behaviour law. As shown in Fig. 4(b), one behaviour law is given for each ZOI of the specimen. This stress calculation technique gives rise to a significant number of behaviour laws per speed loading which correspond to different strain rates caused by the nature of the deformation of the material (heterogeneous). It is then possible to determine the behaviour laws at constant strain rates by cutting the SEĖ surface for a given strain rate (Fig. 5).

The difference between the two ways of calculating the true stress represents the difference between the stress induced by the real and the effective cross-sectional area (i.e, real and effective

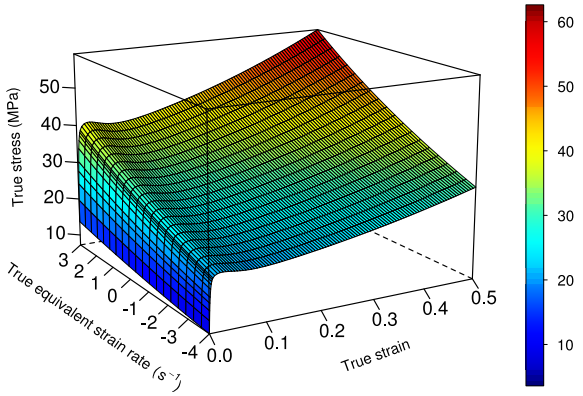

Fig. 5. Surface SEĖ obtained from different ZOI and from tensile tests at different speed loadings.

stress). The damage evolution, resulting from the cavitation process, could then be determined by comparing these two curves. The damage evolution is therefore obtained at constant strain rate by using Eqs. (2) and (3) and 4, by

$$D = 1 - \frac{\sigma_{yy_i}^{\text{com}}}{\sigma_{yy_i}^{\text{inc}}}. \tag{5}$$

In this approach, the damage is therefore obtained by the force evolution which takes the decohesion at the interface particles into account, and the growth of voids which is represented by the effective cross sectional area. The constitutive damage model proposed by Balieu et al. [2,11] is used to fit the observed damage evolution. This damage model is defined such as

$$D = 1 - \exp\left(\frac{\kappa}{k_c}\right), \tag{6}$$

where κ is the equivalent plastic strain and k_c is a material parameter. The unique damage parameter k_c is therefore identified by correlating this evolution with the constitutive damage model by using a least squares optimisation (Fig. 6). This method generates a lot of damage evolutions in each ZOI which cover different strains and strain rates according to the position in the specimen. Finally, the damage evolution law at constant strain rate could be determined. Nevertheless, before validating this method for use with dynamic loading, a comparison must be carried out with the more classical loss of stiffness technique.

2.3. Damage with the loss of stiffness technique

In uniaxial tensile loading, the linear elastic Hooke law, coupled with damage, leads to the expression of the damage according to the loss of stiffness technique [19], given by

$$D = 1 - \frac{\tilde{E}}{E}, \tag{7}$$

where $\tilde{E}$ and E are the Young moduli of the damaged and non-damaged materials, respectively. A uniaxial tensile test with repeated unloadings is therefore used to evaluate the evolution of the damage parameter. For this kind of measurement, Lemaitre [19] recommends the following procedure:

- A specimen with a weakened section in its middle in order to localize the deformation (damage).
- Due to localization of the damage, the deformation needs to be measured by small strain gauges.
- The elasticity modulus is evaluated during the unloading between a lower and upper value of stress in order to eliminate the non-linearity on the stress-strain curve.

The damage measurement of the polymeric material under investigation is carried out with a 5 mm notched specimen in order to localize the deformation in the notch. The Young modulus evolution is obtained by using the displacement in the centre of the specimen (guage length of 2 mm) where the stress triaxiality ratio induced by the geometry effect of the notches could be considered as negligible on this small volume. This uniaxial tensile test with repeated unloading is carried out in quasi-static, the electromagnetic device with a cell force of 3 kN (INSTRON E3000) is therefore used. The specimen is loaded with a prescribed displacement at 1 mm/min for both loadings and unloadings. Some preliminary tests were carried out to evaluate the unloading path in order to avoid the compression loading during the unloading phase of the test. The response of the material in terms of engineering stress-strain is presented in Fig. 7. The expected viscoelastic behaviour with its characteristic hysteresis is clearly captured. Due to the viscoelasticity of the material being studied the loading and unloading phases are not linear. The stiffness is therefore taken between the upper point, at the crossing between loading and unloading curves, and the lower point, at zero stress, of the hysteresis caused by the viscoelastic behaviour. The stiffness evaluated with this method is different to the Young modulus, it is more an indicator of the rigidity. However, for convenience reasons, the term of modulus is employed in this section to designate this rigidity. The loss of stiffness technique is normally used in the unloading part of the curve, but when hysteresis appears, it is difficult to use it as the unloadings are non linear. In consequence, by using the crossing of the loading and unloading curves, the technique could be used with a standard approach to give confident results. The damaged modulus $\tilde{E}$ is evaluated for each hysteresis and the non-damaged modulus E by the first loading path. The complete procedure for the damage measurement by loss of stiffness is summarized in Fig. 8.

The damage variable D is therefore calculated by Eq. (7) for each value of $\tilde{E}$. The evolution of the damage parameter calculated by the loss of stiffness technique versus the true equivalent strain is presented in Fig. 6. In order to compare it with the previous results, the damage evolution characterized with the SEĖ method is plotted on the same Fig. 6. The two evaluation techniques give very close results. As shown with the characterization performed with the SEĖ method, the degradation of the material occurs at the beginning of the deformation.

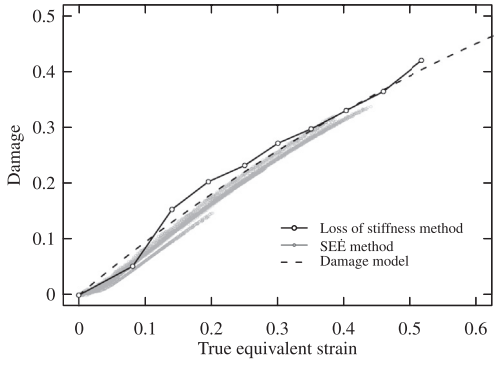

Fig. 6. Comparison of the damage evolution obtained by the loss of stiffness procedure with the SEĖ method.

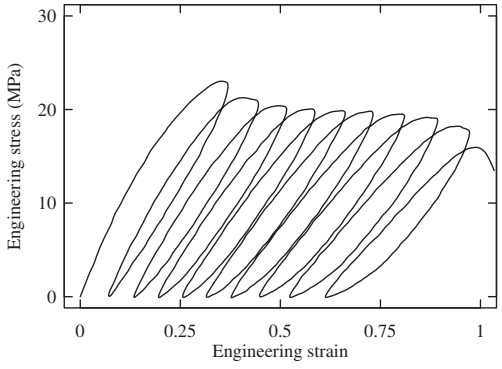

Fig. 7. Engineering stress-strain response obtained by the tensile test with repeated unloading.

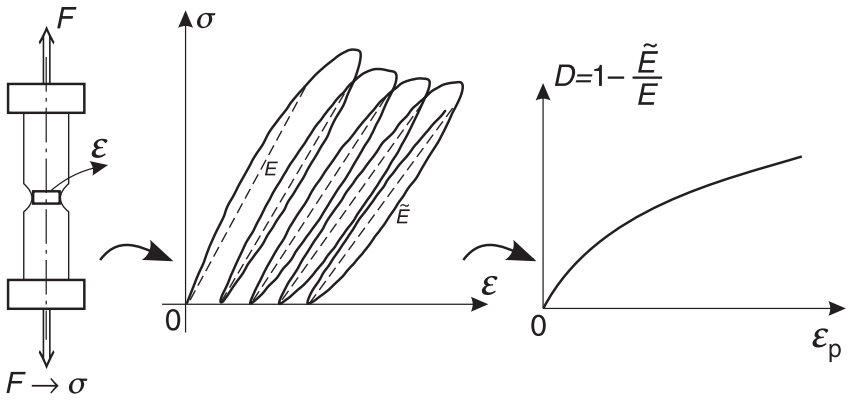

Fig. 8. Procedure for damage measurement by loss of stiffness: 1)Longitudinal strain measurement on notched tensile specimen during loading-unloading, 2) Measurement of an equivalent Young modulus for each hysteresis, 3) Calculation of the damage evolution versus strain.

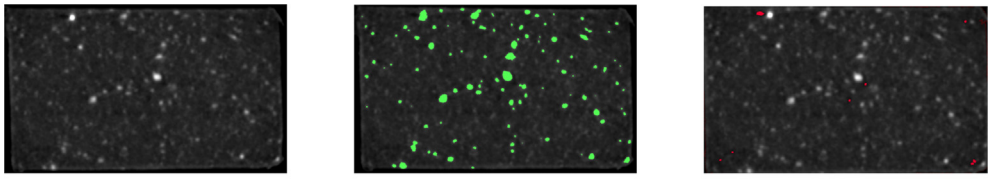

(a) (b) (c)

Fig. 9. Example of a raw grayscale cross section of the specimen in its initial state (a). Talc particles distribution in the initial cross section (green) (b). Voids distribution in the initial cross section (red) (c). (For interpretation of the references to colour in this figure legend, the reader is referred to the web version of this article.)

2.4. Damage observation by microtomography (μCT)

To complete and validate the damage process and in order to visualize the evolution of the damage during the deformation, i.e. the nucleation and growth of voids and cracks, an interrupted in-situ micro tensile test is carried out in an X-ray microtomograph. A small tensile specimen with geometry of 6.35 × 1.78 × 1 mm in the length guage is used. μCT imaging is performed thanks to a 1172 Skyscan system, with 40 kV and 100 μA settings. The voxel size for all μCT data is adjusted to 3.97 μm. This choice ensures capturing small voids size (around 8 μm) with a reasonable imaging duration. Under these conditions, the acquisition of the sample geometry in each mechanical state takes about 8 h. A dedicated in-situ tensile machine developed by Skyscan is mounted on the rotation stage of the tomography set up. In order to avoid blurring the images because of the sample displacement during the scanning, interrupted tests are performed and the motion of the tensile test is stopped before each acquisition. A first μCT-scan is carried out at the initial state (i.e. undamaged material) and two other μCT-scans are performed to follow the evolution of the specimen microstructure at different deformed states. The reconstruction of tomography data leads to a set of grayscale images (Fig. 9(a)) obtained along the principal direction of the sample. Mimics® software is used for thresholding with a selective gray range and transforming each slice to a binary image. The threshold range is chosen to ensure a realistic description of the polymer matrix, talc particles and porosity when it appears (Fig. 9(b) and (c)).

In order to correctly estimate the damage from Eq. (1), an accurate measurement of the cross section of the specimen is necessary. The first use of μCT is to analyse the outer shape of the specimen and how it changed during deformation. The edges of the cross section are detected and the sum of all the pixels leads to the effective cross sectional area S. The real resisting cross sectional area can also be computed by retrieving the void surface (S_D) from the effective cross section area.

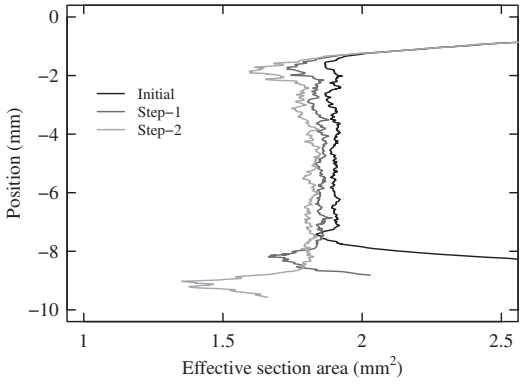

Fig. 10. Evolution of the effective cross sectional area measured by μCT.

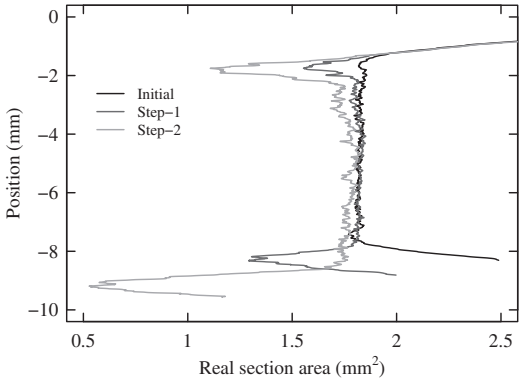

Fig. 11. Evolution of the real cross sectional area measured by μCT.

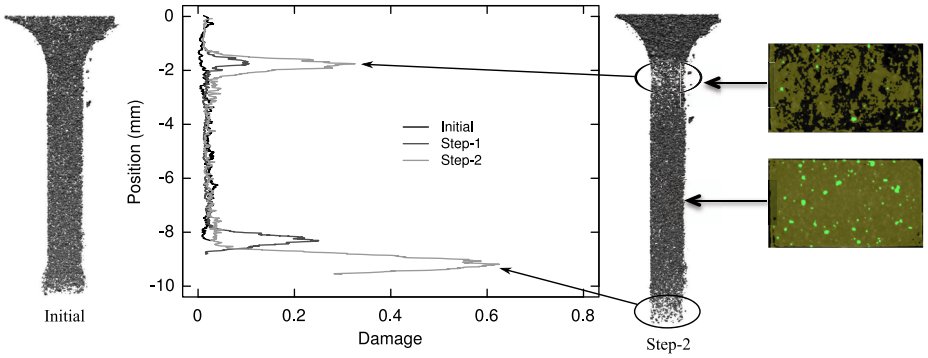

Fig. 12. Evolution of the damage measured by μCT.

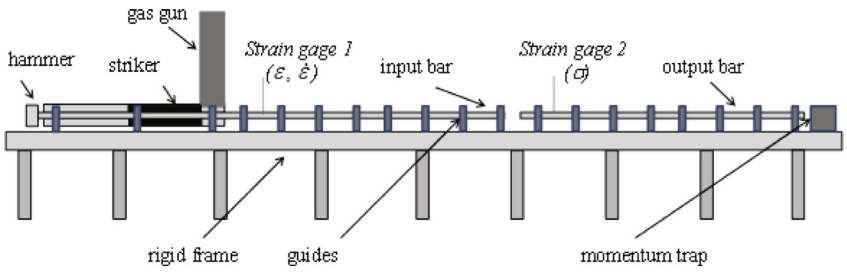

Fig. 13. Schematic of the direct tensile Hopkinson testing.

$$S_{\text{resist}} = S - S_D, \tag{8}$$

The real and effective cross sectional areas along the length guage of the specimen are presented in Figs. 10 and 11 for the initial and two deformed states. In this test, the deformation occurs mainly at the extremities of the length guage. At the bottom of the specimen, where the displacement is applied, the real and effective cross-sectional areas decrease strongly. Another decrease of the two cross sectional areas is observed at the top of the specimen. Recalling the definition of the damage variable in Continuum Damage Mechanics, i.e. Eq. (2), the damage variable evolution is calculated along the length guage of the specimen. The damage evolution during the deformation of the specimen can then be quantified accurately by

$$D = S_{\text{resist}}/S = (S - S_D)/S \tag{9}$$

These results are presented in Fig. 12. No damage occurs in the centre of the specimen between the two localized deformation zones. A rapid increase in the damage, in these two zones, occurs until critical value of 0.6 at the bottom of the specimen. Fig. 12 also includes two cross sectional areas of the deformed specimen, one, in its centre and one in its upper part. The black pixels correspond to the void and the coloured ones include the polymers matrix and the talc fillers. The ratio of void in the presented cross sectional area is 0.38. Comparison of the same cross sectional areas of the specimen before and after deformation in different locations could also confirm the observations. Unfortunately, such a comparison is difficult to make since the deformation is heterogeneous along the specimen and consequently following the exact cross sectional area becomes difficult between two mechanical stages (or scan steps).

The tensile test in-situ X-ray micro-tomography is an interesting technical solution to visualize the evolution of the porosities during deformation. Unfortunately, the localization of the deformations in two very small parts of the specimen makes the deformation measurement difficult. The calculated damage value is therefore, in this case, not accurately correlated to the deformation. Nevertheless, the three techniques converge to an equivalent measurement of the damage evolution and confirm that the SEÈ method is the more efficient one for damage measurement. Another important advantage of this SEÈ method is that it can also be used under dynamic loading conditions without affecting its performance.

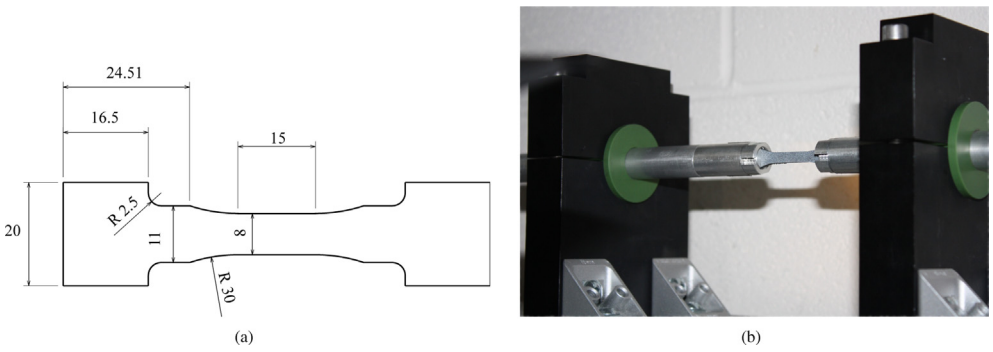

Fig. 14. Hopkinson tensile specimen geometry (a). Hopkinson tensile specimen in the specific clamping device (b).

DOI : 10.1016/j.ijimpeng.2014.08.013

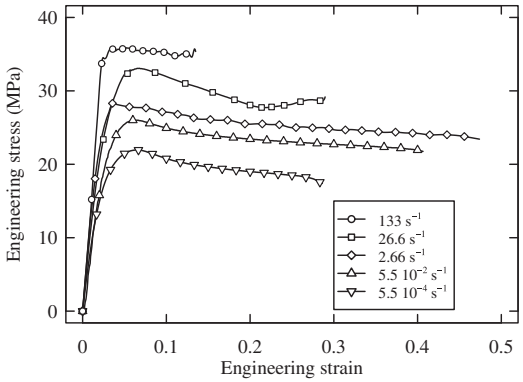

Fig. 15. Stress/strain relationships based on high speed hydraulic machine experiments.

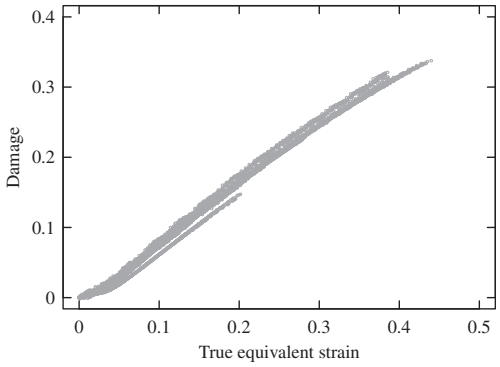

Fig. 17. Damage evolution measured with the SEĖ method for a wide range of strain rates (from low to high strain rates).

3. Damage at moderate and high strain rates

A high speed hydraulic machine (Instron 65 kN-20 m/s) is used for the dynamic loadings. A piezoelectric load cell – calibrated in the range [0; 5] kN with a precision of 25 N – is fixed in the upper part of the machine and an LVDT sensor is used to measure the displacement of the jack during the test. The lower part is composed of the clamping system used to load the specimen once the velocity is constant. The strain rate effects are studied at 0.08, 0.8 and 4 m/s which correspond to average equivalent strain rates of 2.6, 26 and 133 1/s, respectively. Due to ringing phenomenon of the assembly (6 kHz), tensile tests are also performed on direct tensile Hopkinson bars over 200 1/s. This equipment is composed of two aluminium bars made of 6060 Aluminium alloy with 20 mm in diameter and a hollow striker made of Polyamide 66 with respect to impedance matching issues. The cylindrical bars are properly aligned on a rigid frame and have a guiding distance close to 500 mm. The length of the input, output bar and the striker are respectively 5.63, 4 and 1 m. The length of the set bars/striker and the position of the full strain bridges cemented on the bars are chosen with respect to a Lagrangian diagram so as to avoid any superposition of the elastic wavesâ€™ system (Fig. 13).

Each bar is instrumented by a full strain bridge to detect typical incident, reflected and transmitted signals. For these tests, a special specimen with the associated clamping system is proposed with particular attention paid to the distribution of the strain fields (Fig. 14(a) and (b)). The specimen has a reduced guage length to increase strain rate values. Finally, the guage section of the specimen is determined to obtain reflected and transmitted signals of high amplitudes in the range of moderate strain rates.

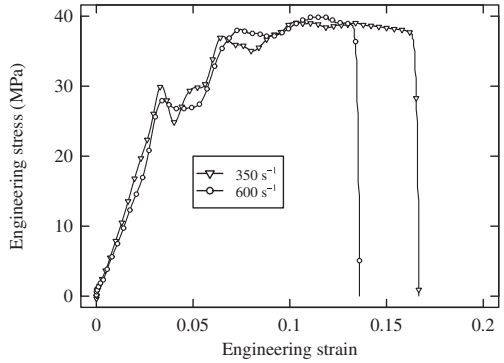

Fig. 16. Stress/strain relationships based on direct tensile Hopkinson testing experiments.

For these tests, two input pressures are used, 9 and 17 bars, which correspond in terms of velocities of the striker to 6.7 and 11.5 m/s. Two approximate strain rates of 350 and 600 1/s can be obtained during the tests with these velocities. The signals given by the strain guages are used with the DAVID® software to obtain the net forces of the tests. For all the tests, the displacements on the specimens are measured by 2D Digital Image Correlation. In Figs. 15 and 16, stress/strain relationships obtained from tensile tests performed on a high speed hydraulic machine and direct tensile Hopkinson bars, respectively, are presented.

By applying the damage measurement with the SEĖ method, the damage evolution obtained for all the tests in each ZOI (static and dynamic) are then plotted in Fig. 17. This result highlights the fact that for this type of semi-crystalline polymer filled with mineral particles, the damage is not strain rate sensitive. That means that the damage constitutive model which will represent this evolution must only be strain dependent. Nevertheless, the fracture strain is strain rate dependent and temperature dependent. For low strain rates, the temperature increases by mechanical deformation and facilitates the molecular chain motion [23], as observed on the tensile tests between $5.5\cdot10^{-4}$ and $5.5\cdot10^{-2}$ (Fig. 15) in which the fracture strain increases. On the contrary, at high strain rates a ductile–fragile transition is observed with low fracture strain [24,25]. For example, in Fig. 15 at $5.5\cdot10^{-2}$ 1/s, the engineering fracture strain is about 0.4 which corresponds to a true equivalent strain of 0.34 and then to a damage value around 0.3 on Fig. 17. For the strain rate of 133 1/s, the engineering fracture strain is about 0.12 (Fig. 15) which corresponds

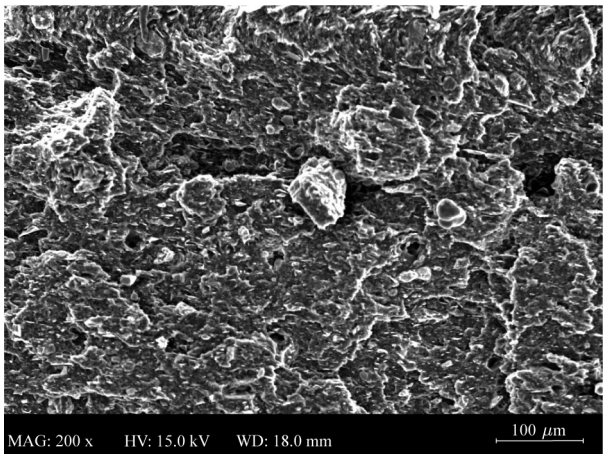

Fig. 18. Fracture surface obtained by magnification SEM micrograph under tensile loading at 600 1/s.

to a true equivalent strain of 0.11 and then to a damage value around 0.1 (Fig. 17). In that case, the macromolecule of the polymer cannot rotate during high strain rate deformation and the rupture occurs earlier in the deformation process. Nevertheless the damage evolution is always the same and mainly controled by decohesion at the interface between the polymer matrix and the mineral particles. This finally leads to different fracture areas, one with long filaments of polymer matrix around particles under static loading and the second one with a flat area representative of a fragile failure under dynamic loading (Figs. 3(b) and 18).

Conclusions

In this paper, the measurement of the damage evolution over a wide strain rate range has been presented. The SEĖ method which was originally developed to measure the behaviour laws on a large strain rate range [16] has been extended in order to measure the damage induced by nucleation, growth and coalescence of cavities. In order to verify the proposed method, several techniques have been presented to evaluate the evolution of the damage variable during deformation. The classic measurement by loss of stiffness technique is compared with the evaluation resulting in the SEĖ method. The two characterization procedures lead to the same damage evolution. The visualization of the porosities by microtomography during an in-situ tensile test has been used to quantify the damage induced by the deformation. Unfortunately, this kind of specimen cannot link the damage variable with a deformation measurement. A uniaxial tensile test in-situ X-ray microtomography with a notched specimen can be a solution to have a better control of the deformation in order to obtain the evolution of the damage variable according to the deformation. However, the results obtained with the various techniques validate the damage measurement with the SEĖ method. This method is then applied with tensile tests under dynamic loading carried out on a hydraulic jack and Hopkinsonâ€™s bars and highlights the independence of the damage evolution at various strain rates for semi-crystalline polymer filled with mineral particles.

Acknowledgements

The present research work has been supported by International Campus on Safety and Intermodality in Transportation, the Région Nord Pas de Calais, the European Community, the Délégation Régionale à la Recherche et à la Technologie, the Ministère de l'Enseignement Supérieur et de la Recherche, and the Centre National de la Recherche Scientifique: the authors gratefully acknowledge the support of these institutions.

References

[1] G'Sell C, Hiver JM, Dahoun A. Experimental characterization of deformation damage in solid polymers under tension, and its interrelation with necking. Int J Solids Struct 2002;39(13–14):3857–72.
[2] Balieu R, Lauro F, Bennani B, Delille R, Matsumoto T, Mottola E. A fully coupled elastoviscoplastic damage model at finite strains for mineral filled semi-crystalline polymer. Int J Plasticity 2013;51:241–70.
[3] Ahzi S, Makradi A, Gregory R, Edie D. Modeling of deformation behavior and strain-induced crystallization in poly(ethylene terephthalate) above the glass transition temperature. Mech Mater 2003;35(12):1139–48.
[4] Ayoub G, Zaïri F, Naït-Abdelaziz M, Gloaguen J. Modelling large deformation behaviour under loading-unloading of semicrystalline polymers: application to a high density polyethylene. Int J Plasticity 2010;26(3):329–47.
[5] Ayoub G, Zaïri F, Frderix C, Gloaguen J, Naït-Abdelaziz M, Seguela R, et al. Effects of crystal content on the mechanical behaviour of polyethylene under finite strains: experiments and constitutive modelling. Int J Plasticity 2011;27(4):492–511.
[6] Nikolov S, Doghri I. A micro/macro constitutive model for the small-deformation behavior of polyethylene. Polymer 2000;41(5):1883–91.
[7] Regrain C, Laiarinandrasana L, Toillon S, Saï K. Multi-mechanism models for semi-crystalline polymer: constitutive relations and finite element implementation. Int J Plasticity 2009;25(7):1253–79.
[8] Krempl E, Khan F. Rate (time)-dependent deformation behavior: an overview of some properties of metals and solid polymers. Int J Plasticity 2003;19(7):1069–95.
[9] Colak OU. Modeling deformation behavior of polymers with viscoplasticity theory based on overstress. Int J Plasticity 2005;21(1):145–60.
[10] Dusunceli N, Colak OU. Modelling effects of degree of crystallinity on mechanical behavior of semicrystalline polymers. Int J Plasticity 2008;24(7):1224–42.
[11] Balieu R, Lauro F, Bennani B, Matsumoto T, Mottola E. Non-associated viscoplasticity coupled with an integral-type nonlocal damage model for mineral filled semi-crystalline polymers. Comput Struct 2014;134:18–31.
[12] Epee A, Lauro F, Bennani B, Bourel B. Constitutive model for a semi-crystalline polymer under dynamic loading. Int J Solids Struct 2011;48(10):1590–9.
[13] Polanco-Loria M, Clausen AH, Berstad T, Hopperstad OS. Constitutive model for thermoplastics with structural applications. Int J Impact Eng 2010;37(12):1207–19.
[14] G'Sell C, Hiver J, Dahoun A, Souahi A. Video-controlled tensile testing of polymers and metals beyond the necking point. J Mater Sci 1992;27(18):5031–9.
[15] G'Sell C, Jonas J. Determination of the plastic behaviour of solid polymers at constant true strain rate. J Mater Sci 1979;14:583–91.
[16] Lauro F, Bennani B, Morin D, Epee A. The SEĖ method for determination of behaviour laws for strain rate dependent material: application to polymer material. Int J Impact Eng 2010;37(6):715–22 [impact Loading of Lightweight Structures].
[17] Addiego F, Dahoun A, G'Sell C, Hiver J-M. Characterization of volume strain at large deformation under uniaxial tension in high-density polyethylene. Polymer 2006;47(12):4387–99.
[18] Zaïri F, Naït-Abdelaziz M, Gloaguen J, Lefebvre J. Modelling of the elasto-viscoplastic damage behaviour of glassy polymers. Int J Plasticity 2008;24(6):945–65.
[19] Lemaitre J. A continuous damage mechanics model for ductile fracture. J Eng Mater Technol 1985;107(1):83–9.
[20] Lauro F, Bennani B, Drazetic P, Oudin J, Ni X. Damage occurrence under dynamic loading for strain rate sensitive materials. Commun Numer Methods Eng 1997;13(7):113–26.
[21] Lauro F, Bennani B, Croix P, Oudin J. Identification of the damage parameters for anisotropic materials by inverse technique: application to an aluminium. J Mater Process Technol 2001;118(13):472–7.
[22] Kachanov L. Time of the rupture process under creep conditions. Izv Akad Nauk USSR Otd Tekh Nauk 1958;8:26–31 [in Russian].
[23] Govaert LE, Engels TAP, Sontjens SHM, Smit TH. Time-dependent failure in load-bearing polymers. A potential hazard in structural applications of polylactides, degradable polymers for skeletal implants. J Mater Sci Mater Med 2008;21:871–8. Springerlink, ISSN: 978-1-60692-426-6.
[24] Furmanski J, Cady CM, Brown EN. Time-temperature equivalence and adiabatic heating at large strains in high density polyethylene and ultra ligh molecular weight polyethylene. Polymer 2013;54:381–90.
[25] Sabin-Chiarilli V, Pabiot J. Transition ductile-fragile des mélanges incompatibles à faibles concentrations à base de polypropylènes recyclé. Eur Polym J 2000;36:1387–99 [in French].